

# Synthesis and Characterization of Two Novel Naphthalenediimide/Zinc Phosphonate Crystalline Materials Precipitated from Different Solvents

Barbra Poly-Anna Vera Melo, Denis Fernando Gregório Junior, Matheus Troilo de Oliveira, Fabiane de Jesus Trindade, Jacco van de Streek, Fabio Furlan Ferreira,\* and Sergio Brochsztain\*



Cite This: *ACS Omega* 2024, 9, 1748–1756



Read Online

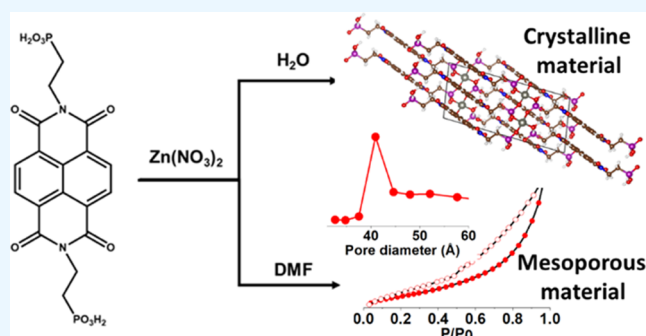
ACCESS |

Metrics & More

Article Recommendations

Supporting Information

**ABSTRACT:** Hybrid naphthalenediimide/zinc phosphonate materials (NDI/Zn) were prepared by mixing solutions of *N,N'*-bis(2-phosphonoethyl)-1,4,5,8-naphthalenediimide (PNDI) and zinc nitrate, resulting in the precipitation of the desired compounds. Samples precipitated from water and *N,N*-dimethylformamide (DMF) were produced. The obtained samples had the expected elemental composition, and the presence of naphthalenediimides (NDI) was ascertained by infrared and UV–visible spectroscopy. All the samples were crystalline, according to powder X-ray diffraction. Nitrogen adsorption isotherms showed the presence of porosity in the NDI/Zn samples. Mesopores with a diameter = 4.1 nm were present in the sample from DMF, with total pore volume reaching 0.13 cm<sup>3</sup>/g.



## INTRODUCTION

Organic metal phosphonates<sup>1–8</sup> constitute a very versatile class of lamellar hybrid materials. Several different metal cations and organic functionalities can be incorporated into metal phosphonates. The organic molecules used as precursors are usually phosphonic or diphosphonic acids, and the most widely employed metal cation is Zr<sup>4+</sup>. Zirconium phosphonates with different organic functionalities have been reported.<sup>1–10</sup> On the other hand, zinc phosphonates have been less explored than their zirconium counterparts. Recently, zinc phosphonates containing different organic functionalities have been reported, employing naphthalene, anthracene, fluorene, and porphyrin diphosphonic acids as precursors.<sup>11,12</sup> Other zinc phosphonate precursors reported in the literature are 4-carboxyphenylphosphonic acid,<sup>13</sup> imidazolylphosphonic acid,<sup>14</sup> and pyridyl, and bipyridyl phosphonic acids.<sup>15–17</sup>

Our research group has been working with naphthalenediimides (NDI), electron-accepting organic compounds often employed as n-type semiconductors in organic electronics.<sup>18–23</sup> We have synthesized *N,N'*-bis(2-phosphonoethyl)-1,4,5,8-naphthalenediimide (PNDI), which is an NDI with two phosphonic acid ligands (Figure 1) and employed it as a precursor for bulk zirconium phosphonate materials, as well as for self-assembled zirconium phosphonate thin films.<sup>10,24–27</sup> To our knowledge, however, there are no reports of zinc phosphonate materials containing naphthalenediimides. In the present report, we describe for the first time the synthesis and characterization of NDI/Zn materials obtained by direct

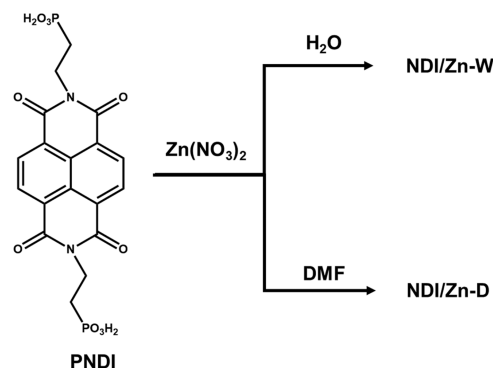


**Figure 1.** Synthesis of NDI/Zn materials by direct precipitation from PNDI and zinc nitrate solutions.

precipitation by mixing solutions of PNDI and zinc nitrate (Figure 1). Recent reports have appeared on the synthesis of NDI-Zn coordination compounds,<sup>28–37</sup> but with other ligands, such as pyridyl,<sup>29–32</sup> pyrazole,<sup>33</sup> tetrazole<sup>34</sup> and isophtha-

**Received:** October 23, 2023

**Revised:** November 28, 2023

**Accepted:** November 30, 2023

**Published:** December 20, 2023



**Table 1. Synthetic Conditions Employed in the Synthesis and Elemental Analysis of the NDI/Zn Samples**

sample	solvent	conditions <sup>a</sup>	drying <sup>a</sup>	% C	% H	% N	formula <sup>b</sup>
NDI/Zn-W	water	7 days, rt, no stirring	vacuum (rt)	37.1	3.25	4.75	PNDI:Zn·2H <sub>2</sub> O
NDI/Zn-D	DMF	48 h, 130 °C, stirring	oven (140 °C)	37.6	3.37	6.24	PNDI:Zn <sub>2</sub> ·DMF

<sup>a</sup>rt: room temperature. <sup>b</sup>Best matching formula (see Table S1).

late,<sup>35,36</sup> rather than phosphonate. The compounds obtained from those NDI precursors, however, formed three-dimensional (3D) metal–organic frameworks, in contrast to phosphonate ligands, which are known to form layered two-dimensional (2D) materials.<sup>38</sup>

## EXPERIMENTAL PART

**Materials.** Zinc nitrate hexahydrate was supplied by Sigma-Aldrich. *N,N'*-Bis(2-phosphonoethyl)-1,4,5,8-naphthalenediimide (PNDI) was synthesized according to the reported method.<sup>10</sup> *N,N'*-Dimethylformamide (DMF), high-performance liquid chromatography (HPLC) degree, was purchased from JT Baker. Deionized water was used for all aqueous solutions.

**Synthesis of NDI/Zn-W.** PNDI (240 mg, 0.50 mmol) was dissolved in 500 mL of hot water (80 °C). 150 mg (0.50 mmol) of Zn(NO<sub>3</sub>)<sub>2</sub>·6H<sub>2</sub>O were added, dissolved in 10 mL of water. A white precipitate was formed while adding the zinc salt. The suspension rested at room temperature (RT) for 7 days when the solid phase settled out. Most of the clear supernatant (400 mL) was decanted, and the rest of the water was separated by centrifugation (5000 rpm). The solid residue was washed with water, centrifuged again, and finally dried under vacuum (24 h at room temperature), giving 233 mg of NDI/Zn-W (75% yield, based on the formula PNDI:Zn·2H<sub>2</sub>O).

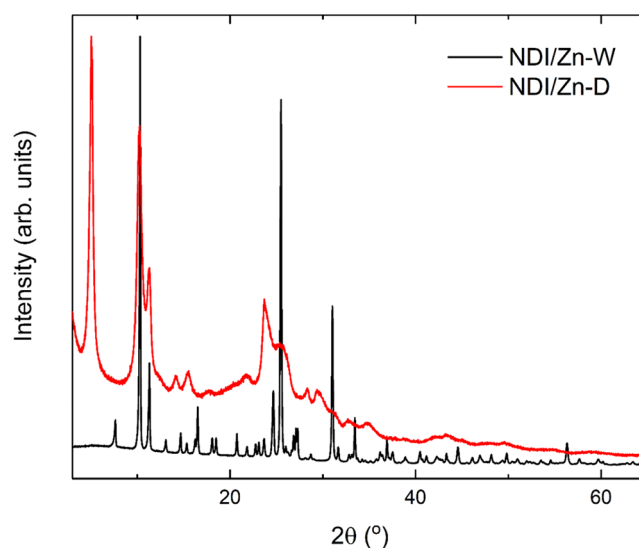
**Synthesis of NDI/Zn-D.** 250 mg of PNDI (0.52 mmol) and 165 mg of Zn(NO<sub>3</sub>)<sub>2</sub>·6H<sub>2</sub>O (0.55 mmol) were mixed with DMF (50 mL). The mixture was heated at 130 °C for 48 h, under stirring, and then allowed to cool down. The resulting solid was vacuum-filtered, washed with DMF (3 times, 5 mL each), and left to dry in a ventilated hood for a week. The solid was finally oven-dried for 48 h at 140 °C, giving 232 mg of NDI/Zn-D (120% yield, based on the formula PNDI:Zn<sub>2</sub>·DMF). The conditions employed to prepare the NDI/Zn samples are summarized in Table 1.

**Instruments.** Solution UV–visible spectra were taken with a Cary-50 spectrophotometer (Varian). Diffuse reflectance spectra (DRS) were also recorded with the Cary-50, using the Barreliño accessory, which features an external optical fiber probe. Nitrogen adsorption isotherms were acquired with a Nova 2200 Surface Area and Pore Size Analyzer (Quantachrome). Specific surface areas were obtained with the Brunauer–Emmett–Teller (BET) method, and pore size distributions (PSD) with the Barrett–Joyner–Halenda (BJH) method (desorption branch). Pore volumes were obtained at  $P/P_0 = 0.97$ . Powder X-ray diffraction measurements were performed on a STADI-P diffractometer, in transmission geometry, using monochromatic Cu K $\alpha_1$  radiation (40 kV, 40 mA) ( $\lambda = 1.54056 \text{ \AA}$ ). A Mythen 1K detector collected data from 3.000 to 97.485° ( $2\theta$ ) in steps of 0.015° and a count time of 100 s at each 1.05°. Elemental analysis (CHN) was carried out at the Analytical Center of the University of Sao Paulo (CA-USP). Infrared spectra were also performed at CA-USP, in a PerkinElmer Frontier FTIR, using KBr pellets. Scanning electron microscopy (SEM) images were

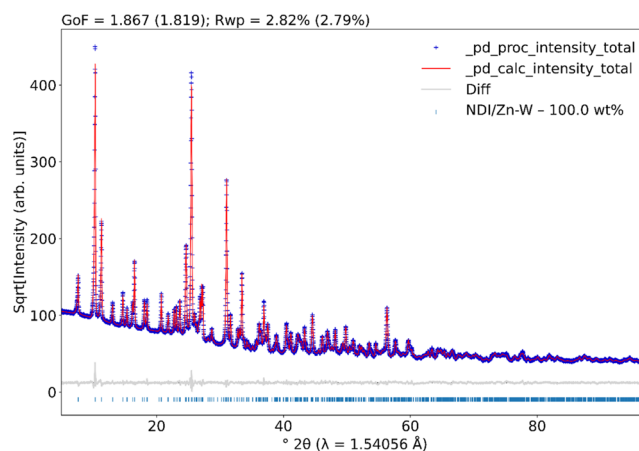
collected with a field emission scanning electron microscope (FESEM) JMS-6701F microscope (JEOL). The NDI/Zn powders were first dispersed in water by sonication. Aliquots of the dispersions (10  $\mu\text{L}$ ) were then transferred to carbon tapes, which were left to dry at room temperature. The samples were then coated with a layer of carbon (3 nm) by sputtering with a Leica EM ACE 200 coating system (diffuse mode).

## RESULTS AND DISCUSSION

**Synthesis of NDI/Zn.** Two different conditions were employed to synthesize NDI/Zn (Table 1). The synthesis in



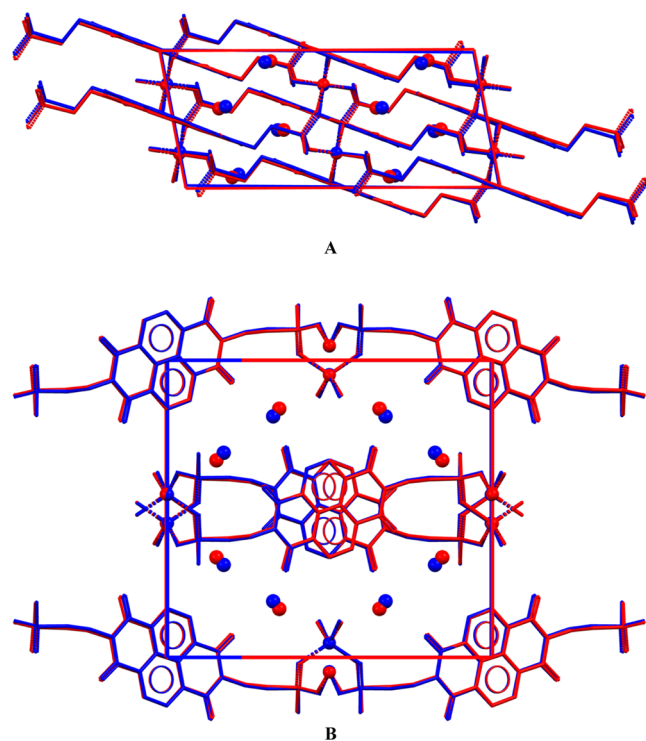
**Figure 2.** Normalized and superimposed powder XRD patterns of NDI/Zn samples precipitated from water (black) and DMF (red).



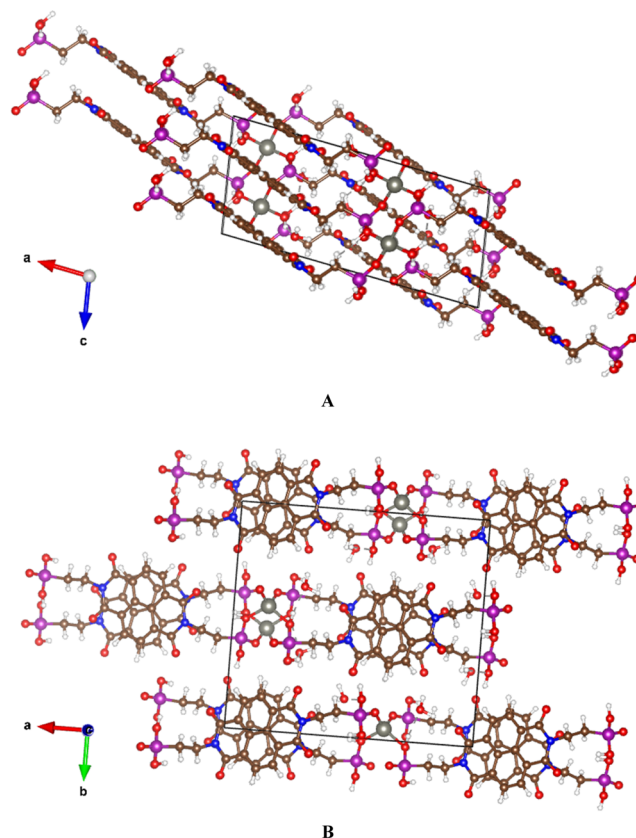
**Figure 3.** Rietveld plot of NDI/Zn-W. The blue crosses indicate the experimental intensities, the red line is the calculated diffractogram based on the determined crystal structure, and the gray line is the difference between the observed and calculated diffractograms. The vertical bars at the bottom indicate the Bragg reflections. For better visualization, the square root of the intensities is plotted.

**Table 2. Crystal Data and Details of the Structure Determination Process of Sample NDI/Zn-W**

chemical formula	$C_{18}H_{14}N_2O_{10}P_2Zn, 2(H_2O)$
formula weight ( $g\ mol^{-1}$ )	581.67
crystal system	monoclinic
space group	$C2/c$ (Nr. 15)
$a, b, c$ (Å)	17.4223(7), 15.6230(8), 7.7560(3)
$\beta$ (deg)	79.4181(10)
volume ( $\text{Å}^3$ )	2075.18(16)
$Z, Z'$	4, 1
$\rho_{\text{calcd}}$ ( $g\ cm^{-3}$ )	1.8619(1)
$T$ (K)	298
Data Collection	
diffractometer	STADI P
monochromator	Ge(111)
wavelength (Å)	1.54056
$2\theta$ range (deg)	3.000–97.485
detector step size (deg)	1.05
time per step (s)	100
data step size (deg)	0.015
Refinement	
number of data points	6300
number of contributing reflections	1023
$R_p$ (%)	2.489
$R_{\text{exp}}$ (%)	1.508
$R_{\text{wp}}$ (%)	2.817
$R_{\text{Bragg}}$ (%)	1.648
$\chi^2$	1.867

**Figure 4.** Overlay of the experimental crystal structure of NDI/Zn-W from Rietveld refinement (red) and after energy minimization with DFT (blue) viewed along the  $b$ -axis (A) and the  $c$ -axis (B). Water molecules and zinc ions are shown as spheres, and hydrogen atoms are omitted for clarity.

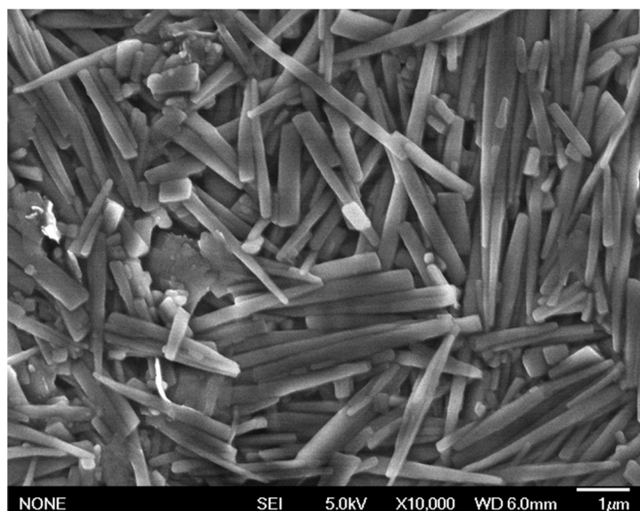
water was performed without stirring, for 7 days at room temperature, in order to ensure a slow precipitation. This

**Figure 5.** Crystal structure of NDI/Zn-W viewed along the  $b$ -axis (A) and the  $c$ -axis (B). Color code: C brown; N blue; O red; H white; P purple; Zn silver.

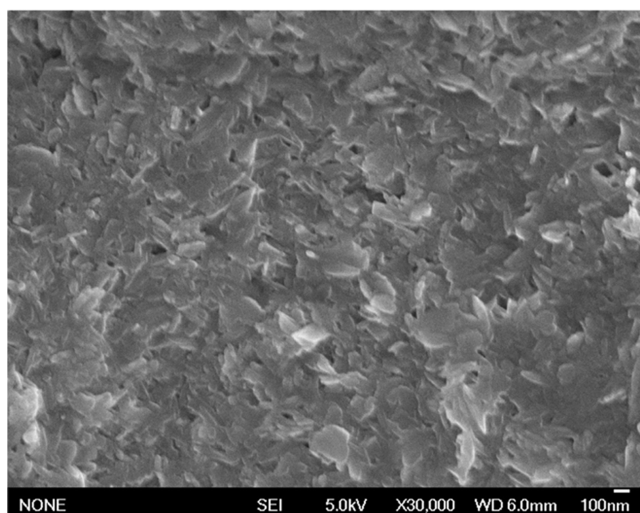
sample, named NDI/Zn-W, was dried under vacuum, at room temperature. The second sample, NDI/Zn-D, was synthesized in hot DMF under stirring for 48 h. The sample was initially dried in air for a week and then in an oven at 140 °C for 48 h. The oven treatment was used to remove the DMF molecules from the materials. However, analysis of NDI/Zn-D before and after the oven treatment showed identical elemental compositions, infrared spectra, and powder XRD (data not shown), indicating that the DMF molecule was not removed in the oven. It can be concluded that a strongly bound lattice DMF was present in NDI/Zn-D.

**Elemental Analysis.** Elemental analyses of the samples are shown in Table 1. Table S1 shows the theoretical composition of different molecular formulas. The elemental composition of NDI/Zn-W is compatible with the formula  $PNDI:Zn \cdot 2H_2O$ , with 1:1 (NDI:Zn) stoichiometry and two lattice water molecules per unit formula, which was confirmed by the XRD data (see below). A reaction yield of 75% was calculated for NDI/Zn-W based on this formula. In the case of NDI/Zn-D, on the other hand, the most likely formula is  $PNDI:Zn_2 \cdot DMF$ , with 1:2 (NDI:Zn) stoichiometry and a lattice DMF molecule. Based on this formula, the reaction yield in the synthesis of NDI/Zn-D was 120%. The XRD data suggests that the excess could be due to contamination with the 1:1 (NDI:Zn) phase.

Based on charge balance, the expected stoichiometry for the materials would be 1:2 (NDI:Zn) since PNDI displays four negative charges (two on each phosphonate group), and therefore, two  $Zn^{2+}$  per unit formula are needed for charge balance. However, the 1:1 stoichiometry is also possible if the



A



B

Figure 6. SEM images of the NDI/Zn materials. (A) NDI/Zn-W. (B) NDI/Zn-D.

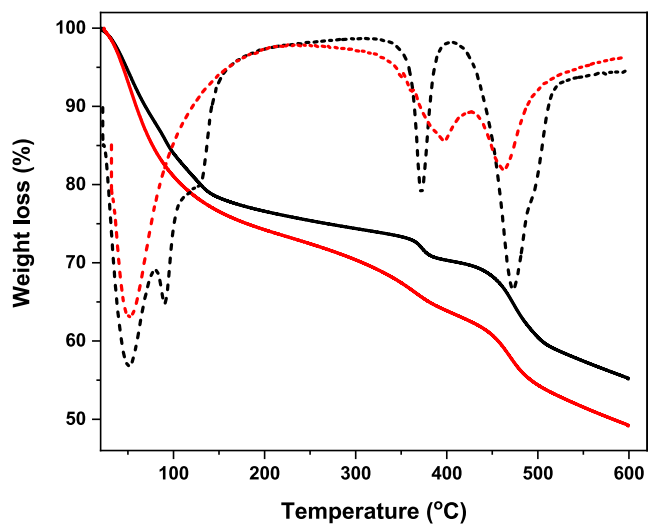
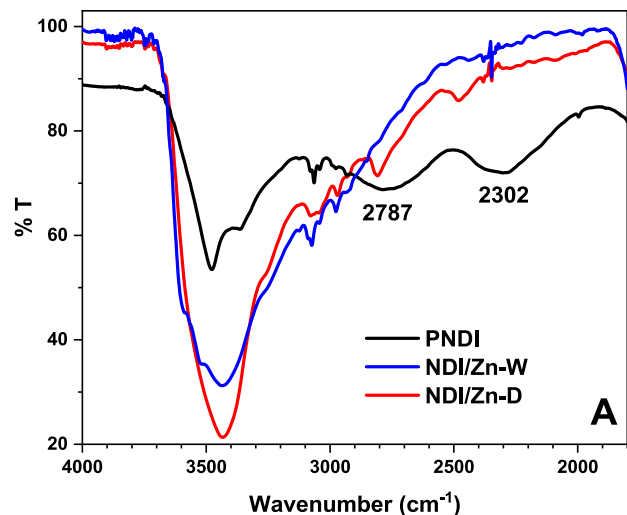
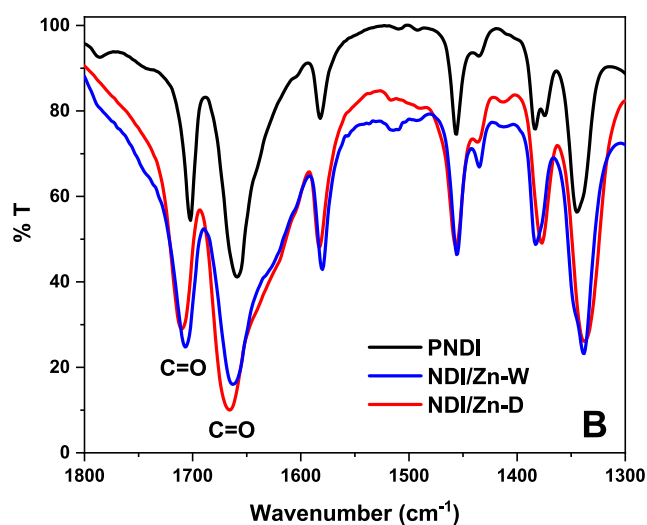


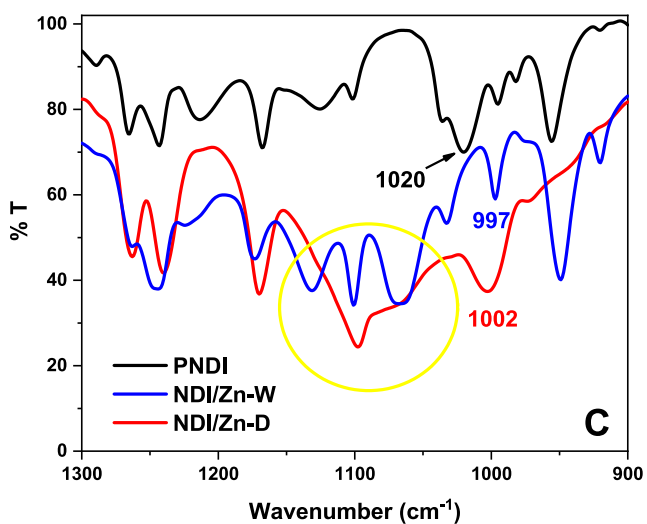
Figure 7. TGA analyses (solid lines) and corresponding DTG plots (dashed lines) for NDI/Zn-W (black) and NDI/Zn-D (red).



A



B



C

Figure 8. Fourier-transform infrared (FTIR) spectra of the NDI/Zn samples, compared to that of pure PNDI (the spectrum of PNDI was offset for clarity). (A) 1800–4000  $\text{cm}^{-1}$  range. (B) 1300–1800  $\text{cm}^{-1}$  range. (C) 900–1300  $\text{cm}^{-1}$  range.

phosphonic acid functionalities are half protonated.<sup>38</sup> The different stoichiometries are consistent with the somewhat

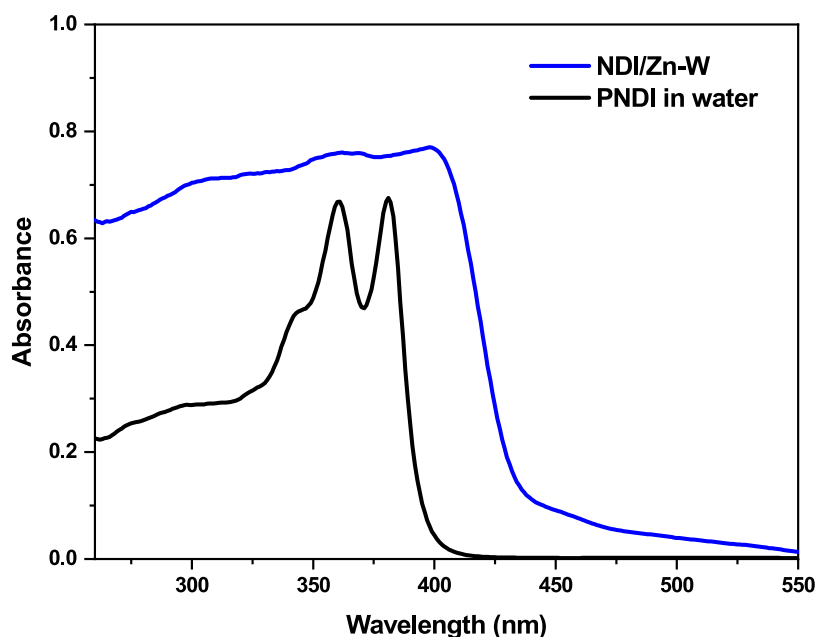


Figure 9. Diffuse reflectance spectrum of NDI/Zn-W and absorption spectrum of PNDI in water.

different crystalline phases found for NDI/Zn-W and NDI/Zn-D by XRD and SEM.

**X-ray Diffraction.** Normalized and superimposed powder XRD patterns of NDI/Zn-W and NDI/Zn-D are shown in Figure 2. The NDI/Zn-W pattern shows sharp and well-defined peaks. On the other hand, the NDI/Zn-D pattern displays broad and overlapped diffraction peaks, which imposes some difficulties in obtaining unequivocal indexing. Due to this limitation, we only describe the indexing procedure for the NDI/Zn-W sample and subsequent crystal structure determination.

The NDI/Zn-W pattern was indexed following some detailed procedures described elsewhere.<sup>39–41</sup> Briefly, we selected the first 20 peaks of the diffraction pattern and used the software TOPAS-Academic v7 to index the pattern.<sup>42</sup> The peak shapes were modeled using a fundamental parameters approach<sup>43</sup> implemented in the TOPAS-Academic v7 software. A full axial model<sup>44</sup> accounted for the axial divergence at low diffraction angles. The background was fitted using a 10th-order Chebyshev polynomial. The sample crystallized in a monoclinic crystal system, and the systematic absences were compatible with space group *Cc*. A Pawley fit was performed, and the refined unit-cell parameters were  $a = 17.4172(7)$  Å,  $b = 15.6243(9)$  Å,  $c = 7.7391(4)$  Å,  $\beta = 100.624(5)^\circ$ , and  $V = 2069.96(18)$  Å<sup>3</sup>. Taking into account the results of the elemental analyses, which indicated a proposed PNDI:Zn·2H<sub>2</sub>O ( $C_{18}H_{16}N_2O_{10}P_2 \cdot Zn \cdot 2H_2O$ ) formula and considering the average volume of the atoms as described by Hofmann,<sup>45</sup> we generated a 3D molecule in MarvinSketch<sup>46</sup> and used it in the DASH software<sup>47</sup> which uses a simulated annealing approach to determine the crystal structure in real space. The full range of possible values (3 degrees of freedom for molecular positions, 4, of which 3 are independent, for orientations, as well as 11 flexible torsion angles) was allowed to vary during the simulated annealing process in a total of  $7.5 \times 10^8$  moves ( $3 \times 10^7$  moves/run, in a total of 25 runs). The best solution was considered for the Rietveld refinement.<sup>48</sup> Figure 3 shows the Rietveld plot obtained using the program *pdCIFplotter*.<sup>49</sup> An eighth-order spherical harmonics accounted

for the preferred orientation of the crystallites. Space groups *Cc* and *C2/c* have the same systematic absences and are, therefore, *a priori* indistinguishable but must be decided between *a posteriori* based on the contents of the unit cell. Using tools like PLATON or CheckCIF<sup>50</sup> to check the crystal geometry, the alternative space group (*C2/c*) was suggested. *C2/c* has twice as many symmetry operators as *Cc*, and the asymmetric unit must, therefore, be halved, i.e., the PNDI molecule must be located on an inversion center, and the zinc ion must be located on a 2-fold rotation axis. The center of mass of the PNDI molecule was moved to the origin, and an inversion center was added to the crystal structure, leading to pairs of overlapping atoms that, in *C2/c*, should be merged. Indeed, all atoms except the two water molecules neatly overlapped and could trivially be merged. The positions of the two water molecules, which after Rietveld refinement in space group *Cc* were 0.6 Å apart, were averaged. The crystal data and details of the structure determination process are displayed in Table 2.

All hydrogen atoms were carefully repositioned so as to form reasonable hydrogen bonds, and the crystal structure was energy minimized with dispersion-corrected density functional theory with FHI-aims.<sup>51</sup> The Perdew–Burke–Ernzerhof functional was used with the nonlocal many-body dispersion correction (PBE-MBD-*nl*). The root-mean-square Cartesian displacement between the experimental structure and the energy-minimized structure (with the unit cell free) was 0.16 Å (Figure 4), indicating that the crystal structure is probably correct.<sup>52</sup>

The water molecules moved considerably upon energy minimization, and they were also the molecules that deviated the most from the *C2/c* symmetry. It is possible that the water molecules are quite mobile in the crystal structure or possibly even disordered, but the correct average space group is *C2/c*, and if the water molecules are disordered, then the experimental structure presented here represents the major occupancy.

The crystal structure of NDI/Zn-W consists of 4 formula units per unit cell ( $Z = 4$ ), accommodating 1 formula unit in the asymmetric unit ( $Z' = 1$ ). The molecules are held together

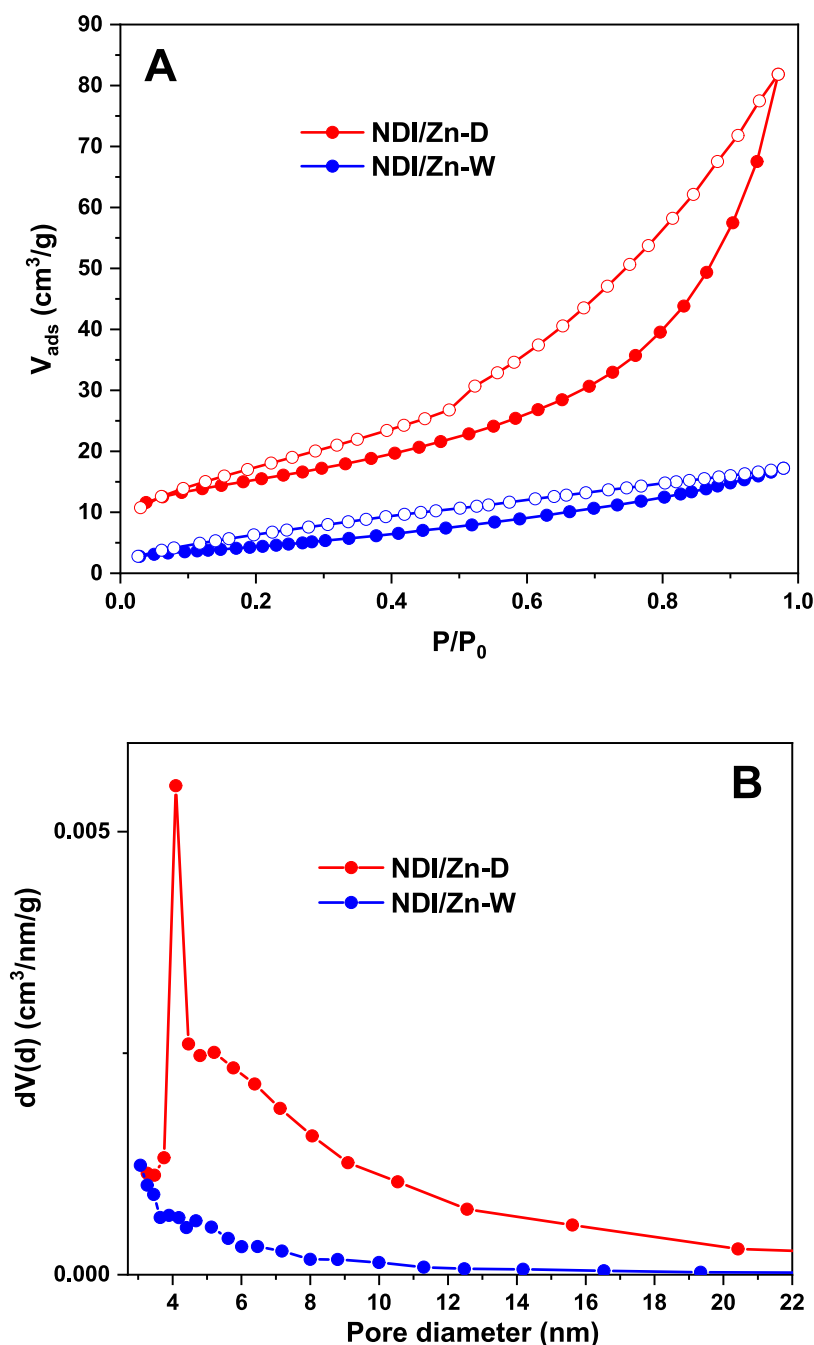


**Figure 10.** (A) Nitrogen adsorption isotherms for NDI/Zn samples. (B) Pore size distributions (BJH method, desorption branch).

**Table 3. Textural Properties of the NDI/Zn Samples**

sample	$S_{\text{BET}}$ (m <sup>2</sup> /g)	$V_p$ (cm <sup>3</sup> /g)	$d$ (nm)
NDI/Zn-W	16	0.027	not detected
NDI/Zn-D	53	0.13	4.1

by  $\pi$ -stacking interactions along the  $b$ -axis and bridging water molecules. Figure 5 shows the crystal structure of the NDI/Zn-W molecule, illustrating some hydrogen interactions and a mean average distance between molecules packed along the  $b$ -axis as being 3.759 Å. The Supporting Information file displays atomic coordinates, bond distances and angles, and hydrogen interactions (Tables S2–S5).

**SEM Images.** Figure 6 shows SEM images of the NDI/Zn materials. The images confirm the results of DRX, showing the

formation of different phases when using different solvents for the synthesis. The sample prepared from water (NDI/Zn-W) displayed long, well-formed rod-like crystals with 2–4  $\mu\text{m}$  lengths and widths of 0.2–0.4  $\mu\text{m}$  (Figure 6A). In the case of NDI/Zn-D, on the other hand, platelet-like crystals were observed, with less defined shapes than in the former case (Figure 6B).

**Thermogravimetric Analysis.** Figure 7 shows the TGA analysis of NDI/Zn-W and NDI/Zn-D, along with the corresponding derivative thermogravimetric (DTG) plots. Both samples showed weight losses at temperatures below 160 °C, corresponding to the loss of solvent molecules, in agreement with the elemental analyses. The organic chains decompose in two steps, with the  $N$ -alkyl chains decomposing between 340 and 400 °C and the aromatic rings in the range

420–530 °C. The final weight losses at 600 °C were between 45 and 50%, corresponding to the sum of C, H, and N (Table 1), suggesting that P, O, and Zn remained in the ashes, perhaps as zinc phosphate.

**Infrared Spectra.** The infrared spectra of the samples are shown in Figure 8, compared with that of pure PNDI. The presence of PNDI in the NDI/Zn materials is ascertained by the coincidence of the spectra, especially in the region from 1300 to 1800  $\text{cm}^{-1}$  (Figure 8B), where the symmetric and asymmetric imide carbonyl bands are found (1650–1710  $\text{cm}^{-1}$ ). These are the most characteristic IR bands of aromatic imides. Aliphatic C–H stretch bands due to the N–CH<sub>2</sub>–CH<sub>2</sub>–P chains are also visible between 2800 and 3000  $\text{cm}^{-1}$  (Figure 8A). The broadband near 3400  $\text{cm}^{-1}$  supports the presence of crystallization water in the NDI/Zn samples.

The main differences between the spectra of PNDI and the NDI/Zn samples are found in the phosphonate-related bands. The two broad bands centered at 2302 and 2787 in PNDI can be attributed to phosphonic acid O–H stretch<sup>53</sup> (Figure 8A). These bands are absent in the NDI/Zn samples, indicating that the phosphonic acids were deprotonated for coordination with Zn<sup>2+</sup>. Furthermore, the phosphonate P–O stretching band, found at 1020  $\text{cm}^{-1}$  in PNDI, was shifted to near 1000  $\text{cm}^{-1}$  in NDI/Zn (Figure 8C), again suggesting coordination with Zn<sup>2+</sup>. New bands were found in the NDI/Zn samples between 1050 and 1150  $\text{cm}^{-1}$ , which are not present in PNDI, that we tentatively assign to the Zn–O stretch.

**UV-visible Spectra.** The diffuse reflectance spectrum of NDI/Zn-W is shown in Figure 9, compared to the spectrum of pure PNDI in an aqueous solution. It was impossible to record the spectrum of NDI/Zn-D (only noise appeared), which we attribute to the highly scattering character of the sample. NDI/Zn-W features an absorption band in the UV (300–400 nm), typical of NDI, in the same region as the absorption band of PNDI in solution. However, the band in the solid was broader than in the solution and without vibrational resolution (Figure 9). Moreover, a shoulder extending between 450 and 550 nm could be due to charge transfer between  $\pi$ -stacked NDI molecules, consistent with the extensive  $\pi$ -stacking observed in the crystal structure (Figure 5). This is desirable for semiconductor applications because the optical band gap was reduced from 3 eV in pure PNDI to 2.3 eV in NDI/Zn-W.

**Nitrogen Adsorption Isotherms.** Nitrogen adsorption isotherms of the NDI/Zn powders are shown in Figure 10A, and the respective textural parameters are given in Table 3. Figure 10B shows the pore size distributions obtained from the isotherms. NDI/Zn-D presented higher surface area and pore volume than NDI/Zn-W. The surface area and pore volume for NDI/Zn-D reached 53  $\text{m}^2/\text{g}$  and 0.13  $\text{cm}^3/\text{g}$ , respectively, similar to other reported zinc phosphonates.<sup>54,55</sup> Furthermore, NDI/Zn-D presented mesoporosity, with well-defined pores with a diameter of 4.1 nm (Figure 10B). The presence of mesoporosity is a desirable feature<sup>56</sup> since it allows the incorporation of several guest species into the material. NDI/Zn-W, on the other hand, presented low porosity without a maximum in the pore size distribution, as expected from the crystal structure (Figure 5). Moreover, micropore analysis using the *t*-plot method (not shown) showed no evidence for the presence of micropores in either of the samples.

## CONCLUSIONS

The NDI/Zn materials described here are fascinating pillared lamellar compounds obtained by a facile precipitation method.

The synthetic methods developed here offer the possibility of tuning the *d*-spacing and the porosity of the materials by the simple choice of solvent. The sample obtained from DMF presented well-defined mesopores, widening the scope of potential applications of the NDI/Zn materials.

## ASSOCIATED CONTENT

### Supporting Information

The Supporting Information is available free of charge at <https://pubs.acs.org/doi/10.1021/acsomega.3c08345>.

Table with the theoretical compositions of the samples for different formulas (Table S1); atomic coordinates of the NDI/Zn-W compound (Table S2); bond lengths for the NDI/Zn-W compound (Table S3); valence angle data for the NDI/Zn-W compound (Table S4); hydrogen-bonding information for the NDI/Zn-W compound (Table S5) (PDF)

## AUTHOR INFORMATION

### Corresponding Authors

Fabio Furlan Ferreira – Center for Natural Sciences and Humanities, Federal University of ABC, 09280-560 Santo André, Brazil; [orcid.org/0000-0003-1516-1221](https://orcid.org/0000-0003-1516-1221); Email: [fabio.furlan@ufabc.edu.br](mailto:fabio.furlan@ufabc.edu.br)

Sergio Brochsztain – Center for Engineering, Modeling and Applied Social Sciences, Federal University of ABC, 09280-560 Santo André, Brazil; [orcid.org/0000-0002-1129-8039](https://orcid.org/0000-0002-1129-8039); Email: [sergio.brochsztain@ufabc.edu.br](mailto:sergio.brochsztain@ufabc.edu.br)

### Authors

Barbra Poly-Anna Vera Melo – Center for Engineering, Modeling and Applied Social Sciences, Federal University of ABC, 09280-560 Santo André, Brazil

Denis Fernando Gregório Junior – Center for Engineering, Modeling and Applied Social Sciences, Federal University of ABC, 09280-560 Santo André, Brazil

Matheus Troilo de Oliveira – Center for Engineering, Modeling and Applied Social Sciences, Federal University of ABC, 09280-560 Santo André, Brazil

Fabiane de Jesus Trindade – Center for Engineering, Modeling and Applied Social Sciences, Federal University of ABC, 09280-560 Santo André, Brazil

Jacco van de Streek – Avant-Garde Materials Simulation, 79249 Merzhausen, Germany

Complete contact information is available at:

<https://pubs.acs.org/doi/10.1021/acsomega.3c08345>

### Notes

The authors declare no competing financial interest.

## ACKNOWLEDGMENTS

S.B. and F.F.F. acknowledge the support of FAPESP (grants: 2016/05496-2, 2023/08771-8, 2023/02259-3 and 2021/03640-7), CNPq (grant: 305601/2019-9), and CAPES (Finance code 001). The authors are grateful to the Multiuser Central Facilities (UFABC) for the experimental support. The crystal structure was deposited in CCDC under No. 2261438.

## REFERENCES

- (1) Cao, G.; Hong, H.-G.; Mallouk, T. E. Layered Metal Phosphates and Phosphonates: From Crystals to Monolayers. *Acc. Chem. Res.* 1992, 25, 420–427.

- (2) Shimizu, G. K. H.; Vaidhyanathan, R.; Taylor, J. M. Phosphonate and sulfonate metal organic frameworks. *Chem. Soc. Rev.* **2009**, *38*, 1430–1449.
- (3) Gagnon, K. J.; Perry, H. P.; Clearfield, A. Conventional and Unconventional Metal–Organic Frameworks Based on Phosphonate Ligands: MOFs and UMOFs. *Chem. Rev.* **2012**, *112*, 1034–1054.
- (4) Bellitto, C.; Bauer, E. M.; Righini, G. Organic–inorganic hybrids: From magnetic perovskite metal(II) halides to multifunctional metal(II) phosphonates. *Coord. Chem. Rev.* **2015**, *289–290*, 123–136.
- (5) Goura, J.; Chandrasekhar, V. Molecular Metal Phosphonates. *Chem. Rev.* **2015**, *115*, 6854–6965.
- (6) Taddei, M.; Costantino, F.; Vivani, R. Robust Metal–Organic Frameworks Based on Tritopic Phosphonoaromatic Ligands. *Eur. J. Inorg. Chem.* **2016**, *2016*, 4300–4309.
- (7) Bao, S.-S.; Qin, M.-F.; Zheng, L.-M. Metal phosphonates incorporating metalloligands: assembly, structures and properties. *Chem. Commun.* **2020**, *56*, 12090.
- (8) Shearan, S. J.; Stock, N.; Emmerling, F.; Demel, J.; Wright, P. A.; Demadis, K. D.; Vassaki, M.; Costantino, F.; Vivani, R.; Sallard, S.; Salcedo, I. R.; Cabeza, A.; Taddei, M. New Directions in Metal Phosphonate and Phosphate Chemistry. *Crystals* **2019**, *9*, 270.
- (9) Vermeulen, L. A.; Snover, J. L.; Sapochak, L. S.; Thompson, M. E. Efficient Photoinduced Charge Separation in Layered Zirconium Viologen Phosphonate Compounds. *J. Am. Chem. Soc.* **1993**, *115*, 11767–11774.
- (10) Brochsztain, S.; Rodrigues, M. A.; Gregoire, J. F.; Demets, G. J. F.; Politi, M. J. Stabilization of naphthalene-1,8:4,5-dicarboximide radicals in zirconium phosphonate solid materials and thin films. *J. Mater. Chem.* **2002**, *12*, 1250–1255.
- (11) Yücesan, G.; Zorlu, Y.; Stricker, M.; Beckmann, J. Metal-organic solids derived from arylphosphonic acids. *Coord. Chem. Rev.* **2018**, *369*, 105–122.
- (12) Bloyet, C.; Rueff, J.-M.; Cardin, J.; Caignaert, V.; Doualan, J.-L.; Lohier, J.-F.; Jaffrès, P.-A.; Raveau, B. Excimer and Red Luminescence Due to Aggregation-Induced Emission in Naphthalene Based Zinc Phosphonate. *Eur. J. Inorg. Chem.* **2018**, *2018*, 3095–3103.
- (13) Li, J.-T.; Cao, D.-K.; Akutagawa, T.; Zheng, L.-M.  $Zn_3(4-OCC_6H_4PO_3)_2$ : A polar metal phosphonate with pillared layered structure showing SHG-activity and large dielectric anisotropy. *Dalton Trans.* **2010**, *39*, 8606–8608.
- (14) Li, Z.; Liu, X.; Ling, Y.; Chen, Z.; Zhou, Y. A two-dimensional zinc Phosphonate: Synthesis, structure and photoluminescence properties. *Inorg. Chem. Commun.* **2017**, *84*, 59–62.
- (15) Ma, K.-R.; Yin, J.-Z.; Hu, H.-Y.; Kan, Y.-H. Syntheses, Structures and Fluorescent Properties of Two Zn(II)-Diphosphonate Coordination Polymers. *J. Clust. Sci.* **2021**, *32*, 875.
- (16) Li, J.-H.; Han, S.-D.; Pan, J.; Xue, Z.-Z.; Wang, G.-M.; Zong-Hua Wang, Z.-H.; Bao, Z.-Z. Template synthesis and photochromism of a layered zinc diphosphonate. *CrystEngComm* **2017**, *19*, 1160–1164.
- (17) Liu, H.-H.; Ma, Y.-J.; Han, S.-D.; Li, J.-H.; Wang, G.-M. Zinc-diphosphonates with extended dipyrindine units: synthesis, structures, in situ reactions, and photochromism. *Dalton Trans.* **2019**, *48*, 3955–3961.
- (18) Bhosale, S. V.; Jani, C. H.; Langford, S. J. Chemistry of Naphthalene Diimides. *Chem. Soc. Rev.* **2008**, *37*, 331–342.
- (19) Al-Kobaisi, M.; Bhosale, S. V.; Latham, K.; Raynor, A. M.; Bhosale, S. V. Functional Naphthalene Diimides: Synthesis, Properties, and Applications. *Chem. Rev.* **2016**, *116*, 11685–11796.
- (20) Kumar, S.; Shukla, J.; Kumar, Y.; Mukhopadhyay, P. Electron-poor arylenediimides. *Org. Chem. Front.* **2018**, *5*, 2254–2276.
- (21) Katz, H. E.; Lovinger, A. J.; Johnson, J.; Kloc, C.; Siegrist, T.; Li, W.; Lin, Y.-Y.; Dodabalapur, A. A Soluble and Air-Stable Organic Semiconductor with High Electron Mobility. *Nature* **2000**, *404*, 478–481.
- (22) Zhan, X.; Facchetti, A.; Barlow, S.; Marks, T. J.; Ratner, M. A.; Wasielewski, M. R.; Marder, S. R. Rylene and Related Diimides for Organic Electronics. *Adv. Mater.* **2011**, *23*, 268–284.
- (23) Nowak-Król, A.; Shoyama, K.; Stolteb, M.; Würthner, F. Naphthalene and perylene diimides—better alternatives to fullerenes for organic electronics? *Chem. Commun.* **2018**, *54*, 13763–13772.
- (24) Rodrigues, M. A.; Petri, D. F. S.; Politi, M. J.; Brochsztain, S. Novel self-assembled films of zirconium phosphonate/1,4,5,8-naphthalenediimides. *Thin Solid Films* **2000**, *371*, 109–113.
- (25) Marcon, R. O.; Brochsztain, S. Characterization of self-assembled thin films of zirconium phosphonate/aromatic diimides. *Thin Solid Films* **2005**, *492*, 30–34.
- (26) Marcon, R. O.; Bonvent, J.-J.; Brochsztain, S. Radical Anions and Dianions of Naphthalenediimides Generated within Layer-by-Layer Zirconium Phosphonate Thin Films. *Langmuir* **2022**, *38*, 2153–2161.
- (27) Marcon, R. O.; Bonvent, J.-J.; Brochsztain, S. Stabilization of free radicals in layer-by-layer nanoarchitectures containing multiple arylenediimides. *Dyes Pigm.* **2022**, *198*, No. 109948.
- (28) Pan, M.; Lin, X.-M.; Li, G.-B.; Su, C.-Y. Progress in the Study of Metal–Organic Materials Applying Naphthalene Diimide (NDI) Ligands. *Coord. Chem. Rev.* **2011**, *255*, 1921–1936.
- (29) Ma, B.-Q.; Mulfort, K. L.; Hupp, J. T. Microporous Pillared Paddle-Wheel Frameworks Based on Mixed-Ligand Coordination of Zinc Ions. *Inorg. Chem.* **2005**, *44*, 4912–4914.
- (30) Mulfort, K. L.; Hupp, J. T. Chemical reduction of metal-organic framework materials as a method to enhance gas uptake and binding. *J. Am. Chem. Soc.* **2007**, *129*, 9604–9605.
- (31) D’Alessandro, D. M. Exploiting redox activity in metal–organic frameworks: concepts, trends and perspectives. *Chem. Commun.* **2016**, *52*, 8957–8971.
- (32) Takashima, Y.; Martínez, V. M.; Furukawa, S.; Kondo, M.; Shimomura, S.; Uehara, H.; Nakahama, M.; Sugimoto, K.; Kitagawa, S. Molecular decoding using luminescence from an entangled porous framework. *Nat. Commun.* **2011**, *2*, No. 168.
- (33) Wade, C. R.; Li, M.; Dinca, M. Facile Deposition of Multicolored Electrochromic Metal–Organic Framework Thin Films. *Angew. Chem., Int. Ed.* **2013**, *52*, 13377–13381.
- (34) Xie, Y.-X.; Zhao, W.-N.; Li, G.-C.; Liu, P.-F.; Han, L. A Naphthalenediimide-Based Metal–Organic Framework and Thin Film Exhibiting Photochromic and Electrochromic Properties. *Inorg. Chem.* **2016**, *55*, 549–551.
- (35) Wang, M.-L.; Fu, C.; Li, L.; Zhang, H. A 2D photochromic zinc-based metal–organic framework with naphthalene diimide-type chromophore. *Inorg. Chem. Commun.* **2018**, *94*, 142–145.
- (36) Zhang, H.-L.; Liao, J.-Z.; Yang, W.; Wu, X.-Y.; Lu, C.-Z. A novel naphthalenediimide-based lanthanide–organic framework with polyoxometalate templates exhibiting reversible photochromism. *Dalton Trans.* **2017**, *46*, 4898–4901.
- (37) Garai, B.; Mallick, A.; Banerjee, R. Photochromic metal–organic frameworks for inkless and erasable printing. *Chem. Sci.* **2016**, *7*, 2195–2200.
- (38) Zhang, B.; Poojary, D. M.; Clearfield, A. Synthesis and Characterization of Layered Zinc Biphenylenebis(phosphonate) and Three Mixed-Component Arylenebis(phosphonate)/Phosphates. *Inorg. Chem.* **1998**, *37*, 1844–1852.
- (39) Ferreira, F. F.; Trindade, A. C.; Antonio, S. G.; Paiva-Santos, C. O. Crystal structure of propylthiouracil determined using high-resolution synchrotron X-ray powder diffraction. *CrystEngComm* **2011**, *13*, 5474–5479.
- (40) Ibiapino, A. L.; Seiceira, R. C.; Pitaluga, A.; Trindade, A. C.; Ferreira, F. F. Structural characterization of form I of anhydrous rifampicin. *CrystEngComm* **2014**, *16*, 8555–8562.
- (41) de Figueiredo, L. P.; Ibiapino, A. L.; Amaral, D. N.; Ferraz, L. S.; Rodrigues, T.; Barreiro, E. J.; Lima, L. M.; Ferreira, F. F. *J. Mol. Struct.* **2017**, *1147*, 226–234.
- (42) Coelho, A. A. TOPAS and TOPAS-Academic: an optimization program integrating computer algebra and crystallographic objects written in C++. *J. Appl. Crystallogr.* **2018**, *51*, 210–218.
- (43) Cheary, R. W.; Coelho, A. A. A fundamental parameters approach to X-ray line-profile fitting. *J. Appl. Crystallogr.* **1992**, *25*, 109–121.

(44) Cheary, R. W.; Coelho, A. A. Axial Divergence in a Conventional X-ray Powder Diffractometer. II. Realization and Evaluation in a Fundamental-Parameter Profile Fitting Procedure. *J. Appl. Crystallogr.* **1998**, *31*, 862–868.

(45) Hofmann, D. W. M. Fast estimation of crystal densities. *Acta Crystallogr., Sect. B: Struct. Sci.* **2002**, *58*, 489–493.

(46) *MarvinSketch*, version 23.4.0-6250; ChemAxon, 2023. <https://chemaxon.com>.

(47) David, W. I. F.; Shankland, K.; van de Streek, J.; Pidcock, E.; Motherwell, W. D. S.; Cole, J. C. DASH: a program for crystal structure determination from powder diffraction data. *J. Appl. Crystallogr.* **2006**, *39*, 910–915.

(48) Rietveld, H. M. A profile refinement method for nuclear and magnetic structures. *J. Appl. Crystallogr.* **1969**, *2*, 65–71.

(49) Rowles, M. R. pdCIFplotter: visualizing powder diffraction data in pdCIF format. *J. Appl. Crystallogr.* **2022**, *55*, 631–637.

(50) Spek, A. L. Single-crystal structure validation with the program PLATON. *J. Appl. Crystallogr.* **2003**, *36*, 7–13.

(51) Blum, V.; Gehrke, R.; Hanke, F.; Havu, P.; Havu, V.; Ren, X.; Reuter, K.; Scheffler, M. Ab initio molecular simulations with numeric atom-centered orbitals. *Comput. Phys. Commun.* **2009**, *180*, 2175–2196.

(52) van de Streek, J.; Neumann, M. A. Validation of Experimental Molecular Crystal Structures with Dispersion-corrected Density Functional Theory Calculations. *Acta Crystallogr., Sect. B: Struct. Sci.* **2010**, *66*, 544–558.

(53) Campos, I. B.; Nantes, I. L.; Rodrigues, F. A.; Brochsztain, S. Photoinduced electron transfer in silica-supported self-assembled thin films containing a 1,4,5,8-naphthalenetetracarboxylic diimide and cytochrome *c*. *J. Mater. Chem.* **2004**, *14*, 54–60.

(54) Poojary, D. M.; Zhang, B.; Bellinghausen, P.; Clearfield, A. Synthesis and X-ray Powder Structures of Covalently Pillared Lamellar Zinc Bis(phosphonates). *Inorg. Chem.* **1996**, *35*, 5254–5263.

(55) Clearfield, A. Organically Pillared Micro- and Mesoporous Materials. *Chem. Mater.* **1998**, *10*, 2801–2810.

(56) Wharmby, M. T.; Mowat, J. P. S.; Thompson, S. P.; Wright, P. A. Extending the Pore Size of Crystalline Metal Phosphonates toward the Mesoporous Regime by Isorecticular Synthesis. *J. Am. Chem. Soc.* **2011**, *133*, 1266–1269.